HHS Public Access

Author manuscript

J Magn Reson Imaging. Author manuscript; available in PMC 2018 September 01.

Published in final edited form as:

J Magn Reson Imaging. 2017 September ; 46(3): 887–896. doi:10.1002/jmri.25613.

Imaging Left-ventricular Mechanical Activation in Heart Failure Patients using Cine DENSE MRI: Validation and Implications for Cardiac Resynchronization Therapy

Daniel A. Auger, Ph.D.[1], **Kenneth C. Bilchick, M.D.**[2], **Jorge A. Gonzalez, M.D.**[2], **Sophia X. Cui, B.S.**[1], **Jeffrey W. Holmes, M.D.,Ph.D.**[1,2], **Christopher M. Kramer, M.D.**[2,3], **Michael Salerno, M.D.,Ph.D.**[1,2], and **Frederick H. Epstein, Ph.D.**[1,3]

[1]Department of Biomedical Engineering, University of Virginia Health System, Charlottesville, Virginia

[2]Medicine/Cardiology/Electrophysiology, University of Virginia Health System, Charlottesville, Virginia

[3]Radiology/Medical Imaging, University of Virginia Health System, Charlottesville, Virginia

Abstract

Purpose—Imaging late mechanical activation may identify effective left-ventricular (LV) pacing sites for cardiac resynchronization therapy (CRT). However, there is variability in defining mechanical activation time, with some studies using the time to peak strain (TPS) and some using the time to the onset of circumferential shortening (TOS). We developed improved methods for imaging mechanical activation and evaluated them in heart failure (HF) patients undergoing CRT.

Methods—We applied active contours to cine displacement encoding with stimulated echoes (DENSE) strain images to detect TOS. Six healthy volunteers underwent MRI at 1.5T, and 50 patients underwent pre-CRT MRI (strain, scar, volumes) and echocardiography, assessment of the electrical activation time (Q-LV) at the LV pacing site, and echocardiography assessment of LV reverse remodeling six months after CRT. TPS at the LV pacing site was measured by DENSE.

Results—The latest TOS was greater in HF patients vs. healthy subjects (112±28ms vs. 61±7ms, $p<0.01$). The correlation between TOS and Q-LV was strong ($r>0.75$; $p<0.001$) and better than between TPS and Q-LV ($r<0.62$; $p\geq0.006$). Twenty-three of 50 patients had the latest activating segment in a region other than the mid-ventricular lateral wall, the most common site for the CRT LV lead. Using a multivariable model, TOS/QRS was significantly associated with LV reverse remodeling even after adjustment for overall dyssynchrony and scar ($p<0.05$), whereas TPS was not ($p=0.49$).

Conclusions—Late activation by cine DENSE TOS analysis is associated with improved LV reverse remodeling with CRT and deserves further study as a tool to achieve optimal LV lead placement in CRT.

[§]**Corresponding author:** Frederick H. Epstein, Ph.D., Professor of Biomedical Engineering, Biomedical Engineering and Biomedical Science Building (MR5), 415 Lane Road, Charlottesville, VA 22908, Phone: 434-982-4100, Fax: 434-982-3870, fhe6b@virginia.edu.

Keywords

DENSE; Strain imaging; cardiac resynchronization therapy; mechanical activation

INTRODUCTION

Disorders of the cardiac conduction system such as left bundle branch block (LBBB) and intrinsic myocardial disease cause regional electrical and mechanical activation delays and dyssynchrony (1). These delays vary from patient to patient and can be modified by myocardial scar (2). Cardiac resynchronization therapy (CRT), a common treatment in heart failure (HF), is used to improve synchrony and thus reduce morbidity and mortality (3–5). However, the nonresponder rate remains high (approximately 40%) using the standard CRT approach (6,7). Pre-procedure cardiac imaging is promising for the identification of more-effective pacing sites that may reduce the nonresponse rate. While multiple studies have established that a high CRT nonresponse rate is strongly associated with scar burden, posterolateral scar, and scar at the LV lead implantation site (8–11), it is also established that ideal LV lead implantation sites would be both free of scar and have delayed mechanical activation (12–14). However, there is variability regarding the definition and computation of mechanical activation time, with some studies using the time to peak strain (TPS) (14), some using the presence or extent of late strain onset (12,15), and some relying on manual adjustment of regions of interest during image analysis (14).

Since electrical depolarization initiates mechanical contraction, detecting the onset of contraction represents a nearly direct method for imaging cardiac activation. Using myocardial tagging to assess the time to the onset of circumferential shortening (TOS), McVeigh and colleagues showed a close linear relationship between TOS and electrical activation time and the ability to detect late-activating regions in paced canines (15). While these studies proved the feasibility of imaging TOS to detect late activation, the methods do not easily translate to clinical imaging due to the lengthy process required for accurate analysis of tagged images.

Cine displacement encoding with stimulated echoes (DENSE) is a newer myocardial strain imaging method (16–18) that encodes tissue displacement into the phase of the MR signal and facilitates rapid strain analysis while maintaining accuracy and reproducibility equivalent to myocardial tagging (19). Cine DENSE has been validated versus tagging for the quantification of mechanical dyssynchrony in canines (20), and mechanical dyssynchrony quantified by cine DENSE in HF patients has been shown to be predictive of CRT response (12). Using preliminary methods for the binary assessment of delayed regional mechanical activation, we have shown that the presence of delayed activation at the CRT LV pacing site imaged using cine DENSE is highly associated with CRT response (12,13).

In the present analysis, we developed methods to automatically perform cine DENSE TOS mapping and applied these methods to consecutive patients enrolled in a clinical CRT study in which they underwent pre-CRT cardiac MRI, assessment of Q-LV (QRS to LV electrogram time) at the LV pacing site during the CRT procedure, and assessment of LV

reverse remodeling based on echocardiography before and after CRT. We tested the hypotheses that, compared to cine DENSE TPS measurements, cine DENSE assessment of TOS at the LV pacing site is more closely associated with the Q-LV at the CRT LV pacing site and with the CRT response based on LV reverse remodeling.

MATERIALS AND METHODS

Cohort Selection

Data were acquired from six healthy volunteers (n = 6) and fifty HF patients (n = 50) in accordance with protocols approved by our Institutional Review Board for Human Subjects Research, with all subjects providing informed consent. All patients met the standard criteria for CRT based on established clinical guidelines (21) and had a glomerular filtration rate of at least 40 ml/min/1.73m^2 in order to receive gadolinium. Of the 50 patients, 26 had ischemic cardiomyopathy defined as heart failure believed to be secondary to ischemic heart disease based on the results of coronary angiography and noninvasive imaging. All patients underwent standard CRT procedures in our institution's electrophysiology laboratory where lead implantation was determined based on operator preference for all patients. Operators were blinded to the MRI results in all but five cases, where MR analysis was completed prior to the CRT procedure. With respect to typical operator preference without MRI guidance, operators tend to initially target a site on the LV free wall corresponding to the largest coronary sinus branch. CRT response was defined as a 15% reduction in the LV end-systolic volume (LVESV) based on echocardiography before and 6 months after CRT (22). The authors were blinded to TPS and TOS when assessing the reduction in LV ESV.

Cardiac MR Protocol

All MR studies in HF patients were performed prior to CRT, as described previously (12). Data were acquired using a 1.5T MR scanner (Avanto, Siemens, Erlangen, Germany) with a four-channel phased-array radiofrequency coil. The imaging protocol included steady-state free precession (SSFP) cine imaging, late-gadolinium enhancement (LGE) and cine DENSE. Cine DENSE was performed in 4 short-axis planes at basal, two mid-ventricular, and apical levels. Cine DENSE parameters included a temporal resolution of 17 ms, pixel size of 2.8 × 2.8 mm^2 and slice thickness = 8 mm. Displacement was encoded in two orthogonal directions and a spiral k-space trajectory was used with 6 interleaves per image. Other parameters included: field of view = 350 × 350 mm^2, displacement encoding frequency k_e = 0.1 cycles/mm, flip angle 15° and echo time = 1.9 ms.

Use of Active Contours to Automatically Compute TOS

Semi-automatic strain analysis methods for cine DENSE have been described previously (18,23,24) and were used to compute regional circumferential strain (E_{cc}) for the cine DENSE images. For each slice, midwall E_{cc} was computed for 18 circumferential segments and for all (30 – 40) cardiac phases. To facilitate the automatic computation of TOS, the spatiotemporal midwall E_{cc} data were arranged into a 2D matrix consisting of N rows and M columns, where N represents the number of spatial segments and M represents the number of cardiac phases. Singular value decomposition (SVD) filtering was applied to denoise the strain matrix while maintaining the main features of the spatiotemporal strain field (25).

SVD of the strain matrix was performed by decomposing E_{cc} as $\mathbf{E_{cc} = USV^*}$, where $\mathbf{S} = \mathrm{diag}(S_1, S_2, S_3, \ldots, S_{\mathbf{r}})$, the columns of **U** are orthonormal spatial basis vectors, the columns of **V** are orthonormal temporal basis vectors, * denotes the conjugate transpose operation and **r** represents the rank of E_{cc}. To balance denoising and preservation of detail, a rank-3 SVD approximation of E_{cc} was used.

For the ECG-triggered cine DENSE sequence, the TOS corresponds to the point in time after system detection of the ECG R-wave where dE_{cc}/dt first transitions from a value near zero to a negative value (15,26). Also, since electrical depolarization originates in the right atrium and propagates through the heart's conduction system, activation is continuous across the LV. Given these considerations, we applied an active contour (27) to the denoised strain matrix to compute the TOS map for a slice, as active contours detect image edges (the 2D spatiotemporal gradient of the strain matrix forms a minimum at the TOS) and maintain spatial continuity.

To iteratively guide the active contour to the TOS solution, we used the 2D gradient of the strain matrix to provide forces of attraction and repulsion. The active contour was initialized to the first cardiac phase for all spatial locations. The TOS map for each slice was defined by the final position of the active contour as a function of LV segment.

The active contour was computed using standard methods (27), where the energy functional of the active contour, *s(p)* was defined as:

$$E_{\text{active contour}} = \int_0^1 E_{\text{active contour}}\left(s\left(p\right)\right)\, dp = \int_0^1 E_{\text{int}}\left(s\left(p\right)\right) + E_{\text{ext}}\left(s\left(p\right)\right)\, dp \quad [1]$$

The internal energy component is given by

$$E_{\text{int}}\left(s\left(p\right)\right) = \frac{1}{2}\left(\alpha\left(p\right)\left|s'\left(p\right)\right|^2 + \beta\left(p\right)\left|s''\left(p\right)\right|^2\right) \quad [2]$$

where α and β are constants controlling the stretch and curvature of the contour, respectively, and where s' and s'' represent the first and second derivatives of s, respectively. The external energy component is the 2D gradient of the strain matrix and is defined as

$$E_{\text{ext}}\left(s\left(p\right)\right) = -\left|\nabla E_{cc}\left(x,t\right)\right|^2 \quad [3]$$

where E_{cc} is the denoised strain, and ∇ denotes the 2D gradient operator. The energy functional of the active contour is minimized iteratively using the gradient descent method to compute a solution for *s(p)*.

The two adjustable parameters α and β of the active contour were tuned using separate data sets not included in this study, and then were held constant for all study datasets. These

parameters were tuned so that the active contour could bend sufficiently to detect late activating segments without oversensitivity to noise. The author (DAA) computing TOS was blinded to the CRT outcomes.

TOS Offset Due to System Delays

The calculation of TOS is referenced to the time of the first image of the sequence of cine DENSE images. To reference TOS to the surface ECG QRS peak instead, we measured the delay through the MR system physiological processing unit (36 ms) and accounted for the time used to execute radiofrequency and gradient pulses prior to data readout (10 ms). Accounting for these times, we added a 46 ms offset in time to the E_{cc}-time curves.

Registration of the CRT LV Lead Position at Fluoroscopy with MRI

Registration between biplane fluoroscopy and MRI was accomplished using a modified version of the o'clock method described by Albertsen et al (28) in which we first determined the standard clock face degrees in the left anterior oblique view and basal-apical distance in the right anterior oblique view according to the method, and then used the procedural coronary venogram to improve registration by identifying the coronary sinus os and the most anterior aspect of the vein. The short-axis angular orientation and basal-apical distance obtained from the Albertsen method were applied directly to the 3D MRI TOS and TPS maps for more accurate registration of the TOS and TPS at the LV lead position. The LV lead was determined to be located in an area of scar if it was within 1 cm of scar or there was scar in the AHA segment corresponding to the lead location.

Comparison of Mechanical and Electrical Activation Times and Assessment of Scar and TPS at the LV Lead Position

During CRT implementation, the time interval from the start of the surface QRS to the peak of the LV electrogram at the LV lead implantation site (Q-LV) was assessed (29), and, using the mapping from fluoroscopy to MRI, Q-LV was compared to TOS and TPS at the lead position. In patients with previous myocardial infarction, criteria for scar tissue was a signal intensity at least 2 standard deviations above the mean signal intensity in remote areas. Scar was manually segmented from LGE images by an experienced author (KCB, CMK, MS) as previously described (17) for the determination of presence of scar at the LV lead position. The LV lead was determined to be located in an area of LGE scar if it was within 1 cm of scar or there was scar in the American Heart Association segment corresponding to the lead location. TPS at the LV lead position was computed as the time corresponding to the minimum value of the Ecc curve at that location. The author (DAA) computing TPS and the author segmenting scar (KCB) were blinded to the CRT outcomes.

Statistics

Statistical analysis was performed using SAS 9.4 (Carey, NC). Categorical variables were characterized by the frequency and percentage, while continuous variables were characterized by the mean and standard deviation, or median and interquartile range. Comparisons between continuous variables were performed using the student's t-test. Correlations between continuous variables were performed using the Pearson's correlation

coefficient *r* after confirmation of normality using the Shapiro-Wilk test. Bland-Altman analysis was used to assess the agreement between measurements of activation time.

Bivariable (bivariate) linear regression was used to evaluate the associations between MRI imaging parameters and CRT response based on the percent change in the LVESV 6 months after CRT, the most commonly used measure of LV reverse remodeling after CRT. Multivariable linear regression was used to evaluate the MRI parameters with the most significant associations with CRT response based on bivariable analysis for CRT response. The MRI parameters evaluated included TOS at the LV lead position, TPS at the LV lead position, scar at the LV lead position, and the circumferential uniformity ratio estimate calculated using singular value decomposition (CURE-SVD) (13). $P<0.05$ was considered statistically significant.

RESULTS

The clinical characteristics of the HF/CRT patients are shown in Table 1.

Quantification of Late Mechanical Activation

Example DENSE Ecc maps at various cardiac phases are shown in Figure 1, illustrating typical spatiotemporal patterns of circumferential shortening in a healthy volunteer and a patient with HF-LBBB. Mechanical dyssynchrony is evident in the HF-LBBB patient, as panels F and G of Figure 1 demonstrate early stretch and late activation in the LV lateral wall (arrow).

Figure 2 illustrates the SVD-denoised strain matrices and corresponding strain-time curves for selected segments for the healthy volunteer and patient shown in Figure 1. The examples show synchronous contraction throughout all LV segments for the healthy volunteer and delayed mechanical activation in the lateral wall for the HF-LBBB patient. Figure 2 also depicts the use of active contours to find late activating segments. Shown on the strain matrix pixels are arrows indicating the 2D spatiotemporal gradient that provides the external energy driving the active contour. The final position of the active contour is displayed as a TOS map as demonstrated in Figure 2C and Figure 2F for the volunteer and HF-LBBB patient. Using these methods, the mean of the latest TOS was greater in HF/CRT patients than healthy volunteers (112 ± 28 ms vs. 61 ± 7 ms, $p < 0.01$).

Comparison of Mechanical and Electrical Activation Times

Figure 3 shows the strong correlations between TOS and Q-LV both for patients who had the LV lead placed in a region without scar (panel A; $r=0.76$, $p < 0.001$) and those who had the LV lead placed in a region with scar (panel B; $r=0.84$; $p<0.001$). We observed a greater TOS when the CRT LV lead was in a region containing scar (Fig 3A vs. Fig 3B), consistent with a scar-mediated delay in electromechanical coupling. Bland-Altman plots (Fig 4 A,B) show good agreement between TOS and Q-LV (both normalized to the QRS duration), with a bias relecting a longer mechanical vs. electrical activation time in patients with scar at the LV lead position. In a multivariable linear model, TOS normalized for QRS duration (standardized estimate 0.668, $p<0.0001$) adjusted for the presence of scar at the LV pacing site (standardized estimate −0.298, $p=0.005$) was strongly correlated with the Q-LV (model

R^2=0.512, p<0.0001). In contrast, correlations between TPS and Q-LV were lower for both groups (r=0.44, p=0.006 for panel C [without scar]; r=0.61, p=0.02 for panel D [with scar]).

Heterogeneity in the Location of the Region of Latest Mechanical Activation and CRT LV Lead Placement

Figure 5, panels A and B, show example bull's eye plots of multislice TOS maps, with Figure 5A showing latest activation in the basal anterolateral wall and Figure 5B showing latest activation in the lateral wall toward the apex of the LV. Figure 5C shows the distribution of the location of the latest activated segment, with 27 patients having the latest activated region in the lateral wall at the mid-ventricular level, and 23 patients having latest activation in other locations. As shown, the location of latest activation can vary both circumferentially and from base to apex in the LV.

TOS normalized by the QRS duration provides a dimensionless parameter with median of 0.54 and range of 0.22–1.0 for the patients in this study. For all patients in the study, Figure 6 shows the TOS at the LV lead location normalized to the QRS duration. As shown, 40%, 34%, and 26% of patients had the LV lead placed in a segment with TOS < 50%, 50–69%, and 70–100% of the QRS duration, respectively, highlighting the potential for improvement with imaging guidance. Similarly, 15%, 15%, 25%, and 45% of patients had the CRT LV lead placed in regions with <40%, 40–59%, 60–79%, and 80–100% of the maximum mechanical delay.

TOS Predicts Post-CRT LV Reverse Remodeling

With respect to CRT response, TOS/QRS was significantly associated with LV reverse remodeling measured as the change in LVESV 6 months after CRT (Table 2 and Table 3). Table 2 shows results of a bivariable linear regression models with key MRI parameters as independent variables and the 6-month percent change in LVESV as the dependent variable. As shown in the table, TOS was much more strongly associated with CRT response than TPS. Table 3 shows results of a multivariable linear regression model for TOS/QRS and CRT response with adjustment for CURE-SVD and scar at the LV lead position. As shown in the table, TOS/QRS was significantly associated with LV reverse remodeling, as were scar at the LV pacing site and CURE-SVD. The coefficients in the models for TOS/QRS were −0.461 (p=0.012) in Table 2 and −0.433 (p=0.0046) in Table 3, indicating that each increment of 0.1 in this parameter (for example, an increase in TOS from 50% to 60% of the QRS duration) would be expected to result in an additional absolute 4.6% or 4.3% reduction in the LVESV with CRT. In contrast, TPS was not associated with the change in LVESV after CRT either before adjustment for CURE-SVD and scar at the LV lead position (p=0.96) or after adjustment (p=0.49) (Table 4).

DISCUSSION

Major Findings

The major findings of this study are (a) TOS can be readily measured noninvasively in heart disease patients using active contours applied to cine DENSE strain data and correlates strongly with the electrical activation time, (b) TOS correlates better than TPS with

electrical activation, (c) there is a delay between mechanical and electrical activation in segments with scar, (d) there is substantial heterogeneity in the location of the latest activating region, defined by TOS, in HF patients referred for CRT, (e) in a substantial number of patients the LV lead is placed in an area with significantly less than the maximal mechanical activation time using the conventional CRT implementation, and (f) TOS/QRS at the LV lead position is an independent predictor of LV reverse remodeling after CRT after adjusting for overall dyssynchrony and presence of scar, whereas TPS is not in this cohort.

Advantages of TOS Versus TPS

While previous studies used TPS to assess mechanical activation (14,30), our data show advantages for TOS with respect to correlation with electrical activation and prediction of CRT response. The causal relationship between electrical depolarization and the onset of contraction provides a direct physiological rationale for using TOS. The strong correlation of TOS and electrical activation observed in patients is consistent with previous results in animal models (26). The advantages of TOS over TPS are reflected in the finding that TOS was strongly associated with post-CRT reverse remodeling, whereas TPS was not.

Heterogeneity in Location of Sites with Late TOS

The predominantly anterolateral, lateral, and inferolateral locations of the mechanically late-activating regions are generally consistent with electrical activation patterns for LBBB (31) and with prior echocardiography TPS findings in a similar patient population (30). However, patient-to-patient heterogeneity within this general region was observed. The heterogeneity in the location of latest activating segments is a possible cause of nonresponse to CRT. Our data confirm that, using standard CRT implementation methods, the LV lead is often placed in a region that is not the latest activated.

Active Contour Methodology

In previous studies TOS was computed for individual regional strain-time curves, independent of position, by fitting the data in time (15). We used active contours to incorporate spatiotemporal continuity into the computation of TOS. This approach is consistent with the intrinsic spatiotemporal smoothness of depolarization and may be advantageous for noisy strain data. The use of active contours to measure TOS prevented the erroneous detection of TOS in regions with scar, as scar regions recoil later in the cardiac cycle, whereas viable late-activating areas contract within the first 300 ms of the cardiac cycle, as a conservative estimate. Using active contours tuned for limited bending, in the present study all TOS values were less than 300 ms and all corresponded to non-scar regions. While we applied one-dimensional active contours to each slice, future improvements could investigate 2D active contours to estimate LV TOS surfaces.

Circumferential vs. Radial Strain

Regarding the choice to use circumferential rather than radial strain in this study, we have previously shown the superiority of DENSE circumferential strain over radial strain for the quantification of dyssynchrony (20), a parameter closely related to mechanical activation time. Also, it has been shown that cine DENSE assessment of circumferential strain is more

reproducible than radial strain (19,32). Furthermore, the finding that circumferential strain performs well for this application makes physiologic sense based on the circumferential orientation of midwall myocardial fibers, as shown by diffusion tensor imaging in a canine model of dyssynchrony (33). Lastly, radial strain is particularly poorly-suited for this application beause HF-CRT patients often have dilated ventricles with decreased wall thickness.

Integration of Mechanical Activation Delay and Scar for Optimal CRT Lead Implantation

In addition to late mechanical activation, LV lead position in relation to scar location has been shown to be associated with CRT response. Scar located in the posterolateral segment or LV free wall has been shown to be associated with a decrease in CRT response (8,9,11). As myocardial scar is not readily excitable (34), pacing over a scar region will lead to a prolonged and fractioned QRS complex (35,36) and is associated with a higher rate of death or HF hospitalization (10). Furthermore, it has been shown that pacing outside the LV free wall scar is associated with better CRT response than pacing over LV free wall scar (10). An ideal location would be free of scar, late activating, and accessible by a coronary vein.

Comparison with Other Methods for Imaging Mechanical Activation

The methods developed in this study compare favorably to other methods for imaging cardiac mechanical activation. Radial displacement of the endocardial border imaged using cine MRI has been used previously to identify late activating regions (37), however the relationship between mechanical and electrical delay was inconsistent using this technique compared to our present results. CMR feature tracking has been investigated for imaging late mechanical activation (38), however this study used TPS, not TOS, as a measure of activation time and feature tracking is known to be accurate for whole-slice strain but inaccurate for assessment of segmental strain (39). Echocardiography has also been evaluated for this purpose (40), but MRI is advantageous because it provides scar burden and distribution, coronary venous imaging, and more reproducible strain data.

Clinical Application and Significance

There are a number of advantages to a strategy based on pre-procedure cardiac MRI versus measuring QLV during the procedure. First, MRI evaluation prior to CRT with the addition of MR coronary sinus venography can show the location of venous anatomy relative to areas of late mechanical activation and scar. Second, there may be a site with optimal TOS that is not available from the coronary sinus branches, such that the QLV would never be assessed at this site, and the maximal QLV assessed from the coronary sinus branches would be different from the non-coronary-venous site with maximal TOS. If the patient were a nonresponder after CRT, because this site could not be accessed, knowledge based on MRI that a better site exists would provide justification for surgical placement of an LV epicardial lead at this site. Third, this methodology could be useful in the future with the expected introduction of leadless LV pacing electrodes, as well as for patients in whom endocardial pacing with a transseptal pacing leading is feasible. Fourth, pre-procedure MRI allows imaging of scar, which is prevalent in over half of our patients referred for CRT. Finally, electromechanical coupling may vary from patient to patient.

The absolute decrease in post-CRT LVESV of about 4.5% for each absolute 10% increase in the TOS/QRS ratio is clinically significant. For example, in a patient with a QRS of 150 ms, a 20% absolute increase in the TOS from 50 to 70% of the QRS duration (75 ms to 105 ms) would be expected to result in an absolute additional 9% reduction in LV reverse remodeling. In this hypothetical example, if the CRT pacing site with a TOS of 75 ms would result in an 8% reduction in LVESV, the site with a TOS of 105 ms would be expected to result in an LVESV reduction of 17%, which would cross the threshold for the accepted cutoff of 15% in LVESV reduction for CRT response. If a TOS of 120 ms could be achieved (TOS-QRS ratio of 80%), the reduction in LVESV would be over 21%. While this is one hypothetical example, we demonstrate in this study that in more than half of patients the LV lead is implanted in a region with TOS less than 60% of QRS, demonstrating significant capacity for improvement by targeting late-activating sites. While these findings do not prove that major improvements can be achieved with MRI guidance, they do provide the rationale for a clinical trial using MRI guidance with cine DENSE TOS mapping, LGE scar imaging, and MR coronary venography (41) to determine optimal LV pacing sites and achieve the maximum possible CRT response.

Limitations

Limitations of this study include that cine DENSE covered approximately 80% of the cardiac cycle. A modified cine DENSE sequence with coverage of the full cardiac cycle is currently under development. Although the temporal resolution of cine DENSE (17 ms) is not currently as high as that of echocardiography, this resolution is still quite good, and was sufficient to yield very strong associations with electrical activation and clinical CRT response. The temporal resolution may be increased in future versions of the pulse sequence. Our measurements of electrical activation were taken at the LV lead location only. Measurement of electrical activation at more locations would provide additional data for validation of cine DENSE TOS mapping, although our approach was chosen to minimize disruption of the CRT procedure. In addition, the proposed method includes the need for an additional MRI study; however, the value added by the extra MRI study may outweigh the disadvantage because of the high-quality strain data, scar data, and coronary venous anatomy provided by MRI. The methods in this paper were evaluated in patients with new CRT implants, such that there is also a need to test applicability of these methods to patients requiring CRT upgrades. This should be feasible as the use of MRI in patients with MR-conditional pacemakers and ICDs will increase in the immediate future, and methods to overcome MRI artifacts during cardiac imaging in patients with devices are now available and undergoing optimization. We recognize that there may be limitations regarding registration of the LV lead position between fluoroscopy and MRI (42). Specifically, the orientation and degree of rotation of the heart may vary from patient to patient, and there can be significant interobserver variability among physicians regarding how biplane fluoroscopy of the LV leads is interpreted.

In conclusion, this study demonstrates a robust methodology for cardiac MRI mapping of LV mechanical activation in CRT patients that is more strongly associated with CRT response and electrical activation than measures based on regional time to peak strain. Our

results provide data showing that a randomized prospective CRT clinical trial based on MRI guidance is warranted.

Acknowledgments

Funding support

AHA Grant-in-Aid 12GRNT12050301; Siemens Healthcare - Erlangen, Germany; NIH RO1 EB 001763

Abbreviations and Acronyms

CRT	cardiac resynchronization therapy
HF	heart failure
DENSE	Displacement encoding with stimulated echoes
LGE	Late gadolinium enhancement
LVESV	Left ventricular end systolic volume
LBBB	Left bundle branch block
Q-LV	Electrical activation time
$\mathbf{E_{cc}}$	Circumferential strain
TOS	Time to the onset of circumferential shortening
TPS	Time to peak strain
SVD	Singular value decomposition
CURE	Circumferential uniformity ratio estimate

References

1. Vogler J, Breithardt G, Eckardt L. Bradyarrhythmias and conduction blocks. Revista Española de Cardiología (English Edition). 2012; 65:656–667.
2. Stevenson W, Khan H, Sager P, et al. Identification of reentry circuit sites during catheter mapping and radiofrequency ablation of ventricular tachycardia late after myocardial infarction. Circulation. 1993; 88:1647–1670. [PubMed: 8403311]
3. Abraham WT, Fisher WG, Smith AL, et al. Cardiac resynchronization in chronic heart failure. New England Journal of Medicine. 2002; 346:1845–1853. [PubMed: 12063368]
4. Lindenfeld J, Feldman AM, Saxon L, et al. Effects of cardiac resynchronization therapy with or without a defibrillator on survival and hospitalizations in patients with New York Heart Association class IV heart failure. Circulation. 2007; 115:204–212. [PubMed: 17190867]
5. Moss AJ, Hall WJ, Cannom DS, et al. Cardiac-resynchronization therapy for the prevention of heart-failure events. New England Journal of Medicine. 2009; 361:1329–1338. [PubMed: 19723701]
6. Chung ES, Leon AR, Tavazzi L, et al. Results of the Predictors of Response to CRT (PROSPECT) trial. Circulation. 2008; 117:2608–2616. [PubMed: 18458170]
7. Exner DV, Auricchio A, Singh JP. Contemporary and future trends in cardiac resynchronization therapy to enhance response. Heart rhythm. 2012; 9:S27–S35. [PubMed: 22521939]

8. Bleeker GB, Kaandorp TAM, Lamb HJ, et al. Effect of Posterolateral Scar Tissue on Clinical and Echocardiographic Improvement After Cardiac Resynchronization Therapy. Circulation. 2006; 113:969–976. [PubMed: 16476852]
9. Chalil S, Foley PWX, Muyhaldeen SA, et al. Late gadolinium enhancement-cardiovascular magnetic resonance as a predictor of response to cardiac resynchronization therapy in patients with ischaemic cardiomyopathy. Europace. 2007; 9:1031–1037. [PubMed: 17933857]
10. Chalil S, Stegemann B, Muhyaldeen S, et al. Effect of posterolateral left ventricular scar on mortality and morbidity following cardiac resynchronization therapy. Pacing and Clinical Electrophysiology. 2007; 30:1201–1209. [PubMed: 17897122]
11. White JA, Yee R, Yuan X, et al. Delayed Enhancement Magnetic Resonance Imaging Predicts Response to Cardiac Resynchronization Therapy in Patients With Intraventricular Dyssynchrony. Journal of the American College of Cardiology. 2006; 48:1953–1960. [PubMed: 17112984]
12. Bilchick KC, Kuruvilla S, Hamirani Y, et al. Impact of mechanical activation, scar, and electrical timing on cardiac resynchronization therapy response and clinical outcomes. J Am Coll Cardiol. 2014; 63:1657–1666. [PubMed: 24583155]
13. Ramachandran R, Chen X, Kramer CM, Epstein FH, Bilchick KC. Singular Value Decomposition Applied to Cardiac Strain from MR Imaging for Selection of Optimal Cardiac Resynchronization Therapy Candidates. Radiology. 2015; 275:413–420. [PubMed: 25581423]
14. Saba S, Marek J, Schwartzman D, et al. Echocardiography-guided left ventricular lead placement for cardiac resynchronization therapy: results of the Speckle Tracking Assisted Resynchronization Therapy for Electrode Region trial. Circ Heart Fail. 2013; 6:427–434. [PubMed: 23476053]
15. Wyman BT, Hunter WC, Prinzen FW, McVeigh ER. Mapping propagation of mechanical activation in the paced heart with MRI tagging. American Journal of Physiology-Heart and Circulatory Physiology. 1999; 276:H881–H891.
16. Aletras AH, Ding S, Balaban RS, Wen H. DENSE: displacement encoding with stimulated echoes in cardiac functional MRI. Journal of Magnetic Resonance. 1999; 137:247–252. [PubMed: 10053155]
17. Kim D, Gilson WD, Kramer CM, Epstein FH. Myocardial Tissue Tracking with Two-dimensional Cine Displacement-encoded MR Imaging: Development and Initial Evaluation 1. Radiology. 2004; 230:862–871. [PubMed: 14739307]
18. Spottiswoode BS, Zhong X, Hess A, et al. Tracking myocardial motion from cine DENSE images using spatiotemporal phase unwrapping and temporal fitting. Medical Imaging, IEEE Transactions on. 2007; 26:15–30.
19. Young AA, Li B, Kirton RS, Cowan BR. Generalized spatiotemporal myocardial strain analysis for DENSE and SPAMM imaging. Magnetic Resonance in Medicine. 2012; 67:1590–1599. [PubMed: 22135133]
20. Budge LP, Helms AS, Salerno M, Kramer CM, Epstein FH, Bilchick KC. MR cine DENSE dyssynchrony parameters for the evaluation of heart failure: comparison with myocardial tissue tagging. JACC: Cardiovascular Imaging. 2012; 5:789–797. [PubMed: 22897992]
21. Tracy CM, Epstein AE, Darbar D, et al. 2012 ACCF/AHA/HRS focused update of the 2008 guidelines for device-based therapy of cardiac rhythm abnormalities: a report of the American College of Cardiology Foundation/American Heart Association Task Force on Practice Guidelines. J Am Coll Cardiol. 2012; 60:1297–1313. [PubMed: 22975230]
22. Foley PW, Leyva F, Frenneaux MP. What is treatment success in cardiac resynchronization therapy? Europace. 2009; 11:v58–v65. [PubMed: 19861392]
23. Gilliam AD, Epstein FH. Automated motion estimation for 2-D cine DENSE MRI. Medical Imaging, IEEE Transactions on. 2012; 31:1669–1681.
24. Spottiswoode BS, Zhong X, Lorenz CH, Mayosi BM, Meintjes EM, Epstein FH. Motion-guided segmentation for cine DENSE MRI. Medical image analysis. 2009; 13:105–115. [PubMed: 18706851]
25. Andrews HC, Patterson CL. Singular value decompositions and digital image processing. Acoustics, Speech and Signal Processing, IEEE Transactions on. 1976; 24:26–53.

26. Faris OP, Evans FJ, Ennis DB, et al. Novel technique for cardiac electromechanical mapping with magnetic resonance imaging tagging and an epicardial electrode sock. Annals of Biomedical Engineering. 2003; 31:430–440. [PubMed: 12723684]
27. Kass M, Witkin A, Terzopoulos D. Snakes: Active contour models. International journal of computer vision. 1988; 1:321–331.
28. Albertsen AE, Nielsen JC, Pedersen AK, Hansen PS, Jensen HK, Mortensen PT. Left ventricular lead performance in cardiac resynchronization therapy: impact of lead localization and complications. Pacing Clin Electrophysiol. 2005; 28:483–488. [PubMed: 15955178]
29. Gold MR, Birgersdotter-Green U, Singh JP, et al. The relationship between ventricular electrical delay and left ventricular remodelling with cardiac resynchronization therapy. Eur Heart J. 2011; 32:2516–2524. [PubMed: 21875862]
30. Tanaka H, Hara H, Saba S, Gorcsan J III. Usefulness of three-dimensional speckle tracking strain to quantify dyssynchrony and the site of latest mechanical activation. The American journal of cardiology. 2010; 105:235–242. [PubMed: 20102925]
31. Strik M, Regoli F, Auricchio A, Prinzen F. Electrical and mechanical ventricular activation during left bundle branch block and resynchronization. Journal of cardiovascular translational research. 2012; 5:117–126. [PubMed: 22311563]
32. Lin K, Meng L, Collins JD, Chowdhary V, Markl M, Carr JC. Reproducibility of cine displacement encoding with stimulated echoes (DENSE) in human subjects. Magnetic Resonance Imaging. 2017; 35:148–153. [PubMed: 27569367]
33. Helm PA, Younes L, Beg MF, et al. Evidence of structural remodeling in the dyssynchronous failing heart. Circ Res. 2006; 98:125–132. [PubMed: 16339482]
34. Tedrow U, Maisel WH, Epstein LM, Soejima K, Stevenson WG. Feasibility of adjusting paced left ventricular activation by manipulating stimulus strength. Journal of the American College of Cardiology. 2004; 44:2249–2252. [PubMed: 15582325]
35. Reddy VY, Wrobleski D, Houghtaling C, Josephson ME, Ruskin JN. Combined Epicardial and Endocardial Electroanatomic Mapping in a Porcine Model of Healed Myocardial Infarction. Circulation. 2003; 107:3236–3242. [PubMed: 12796129]
36. Schwartzman D, Chang I, Michele JJ, Mirotznik MS, Foster KR. Electrical Impedance Properties of Normal and Chronically Infarcted Left Ventricular Myocardium. Journal of Interventional Cardiac Electrophysiology. 1999; 3:213–224. [PubMed: 10490477]
37. Suever JD, Hartlage GR, Magrath IIIRP, Iravanian S, Lloyd MS, Oshinski JN. Relationship between mechanical dyssynchrony and intra-operative electrical delay times in patients undergoing cardiac resynchronization therapy. Journal of Cardiovascular Magnetic Resonance. 2014; 16:1. [PubMed: 24387349]
38. Taylor RJ, Umar F, Panting JR, Stegemann B, Leyva F. Left ventricular lead position, mechanical activation, and myocardial scar in relation to left ventricular reverse remodeling and clinical outcomes after cardiac resynchronization therapy: A feature-tracking and contrast-enhanced cardiovascular magnetic resonance study. Heart Rhythm. 2016; 13:481–489. [PubMed: 26498258]
39. Cowan BR, Peereboom SM, Greiser A, Guehring J, Young AA. Image Feature Determinants of Global and Segmental Circumferential Ventricular Strain From Cine CMR. JACC: Cardiovascular Imaging. 2015; 8:1465–1466. [PubMed: 25577442]
40. Khan FZ, Virdee MS, Palmer CR, et al. Targeted Left Ventricular Lead Placement to Guide Cardiac Resynchronization TherapyThe TARGET Study: A Randomized, Controlled Trial. Journal of the American College of Cardiology. 2012; 59:1509–1518. [PubMed: 22405632]
41. Lam A, Mora-Vieira LF, Hoskins M, Lloyd M, Oshinski JN. Performance of 3D, navigator echo-gated, contrast-enhanced, magnetic resonance coronary vein imaging in patients undergoing CRT. Journal of Interventional Cardiac Electrophysiology. 2014; 41:155–160. [PubMed: 25227865]
42. Sommer A, Kronborg MB, Nørgaard BL, Gerdes C, Mortensen PT, Nielsen JC. Left and right ventricular lead positions are imprecisely determined by fluoroscopy in cardiac resynchronization therapy: a comparison with cardiac computed tomography. Europace. 2014; 16:1334–1341. [PubMed: 24687965]

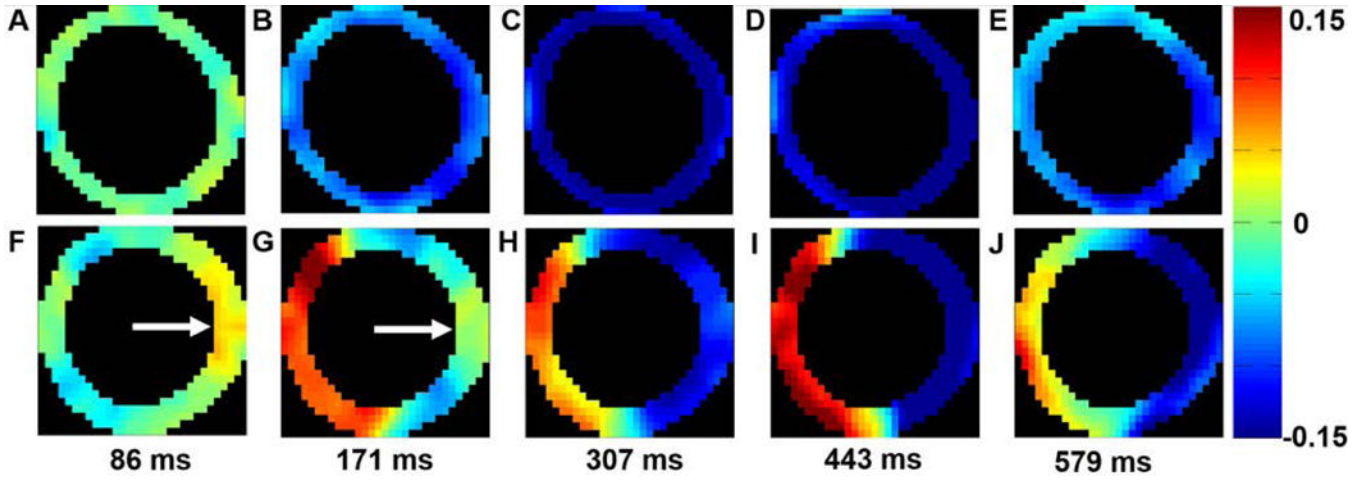

Figure 1. Spatiotemporal patterns of mechanical activation

Five time points distributed across the cardiac cycle show typical spatiotemporal patterns of circumferential shortening in a healthy volunteer (A–E) and a patient with HF-LBBB (F – J). (A –E) illustrate a synchronous contraction for all LV segments. In contrast, (F – J) illustrate dyssynchrony, as contraction and stretch occur simultaneously. The white arrows in (F, G) show a region of late mechanical activation in the lateral wall during early systole.

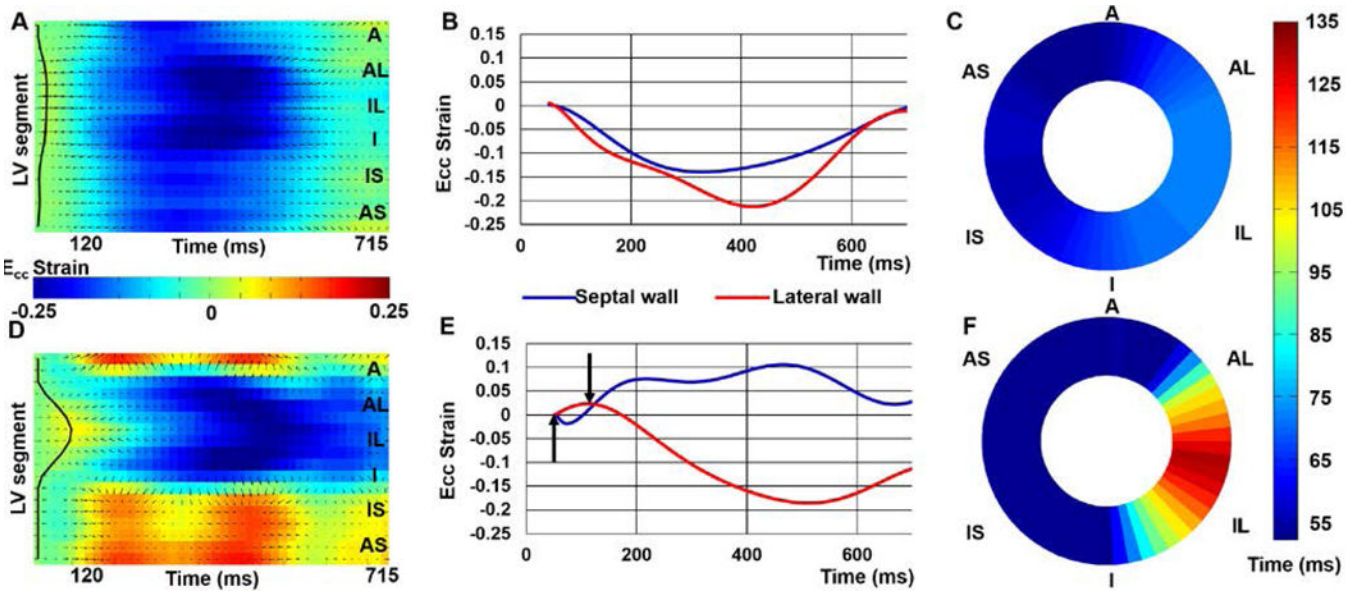

Figure 2. Analysis of late mechanical activation

SVD-denoised strain matrices, E_{cc}-time curves and DENSE mechanical activation time maps are shown for a healthy volunteer (A – C) and a HF/CRT patient (D – E). Panels (A–C) correspond to the healthy volunteer and demonstrate synchrony of contraction, detection of the activation times using the active contour, and early mechanical activation throughout the entire slice. In contrast, panels (D–E) show a region of pre-stretch and late activation, detection of the late-activating region by the active contour, and an activation time map depicting late activation of the lateral wall.

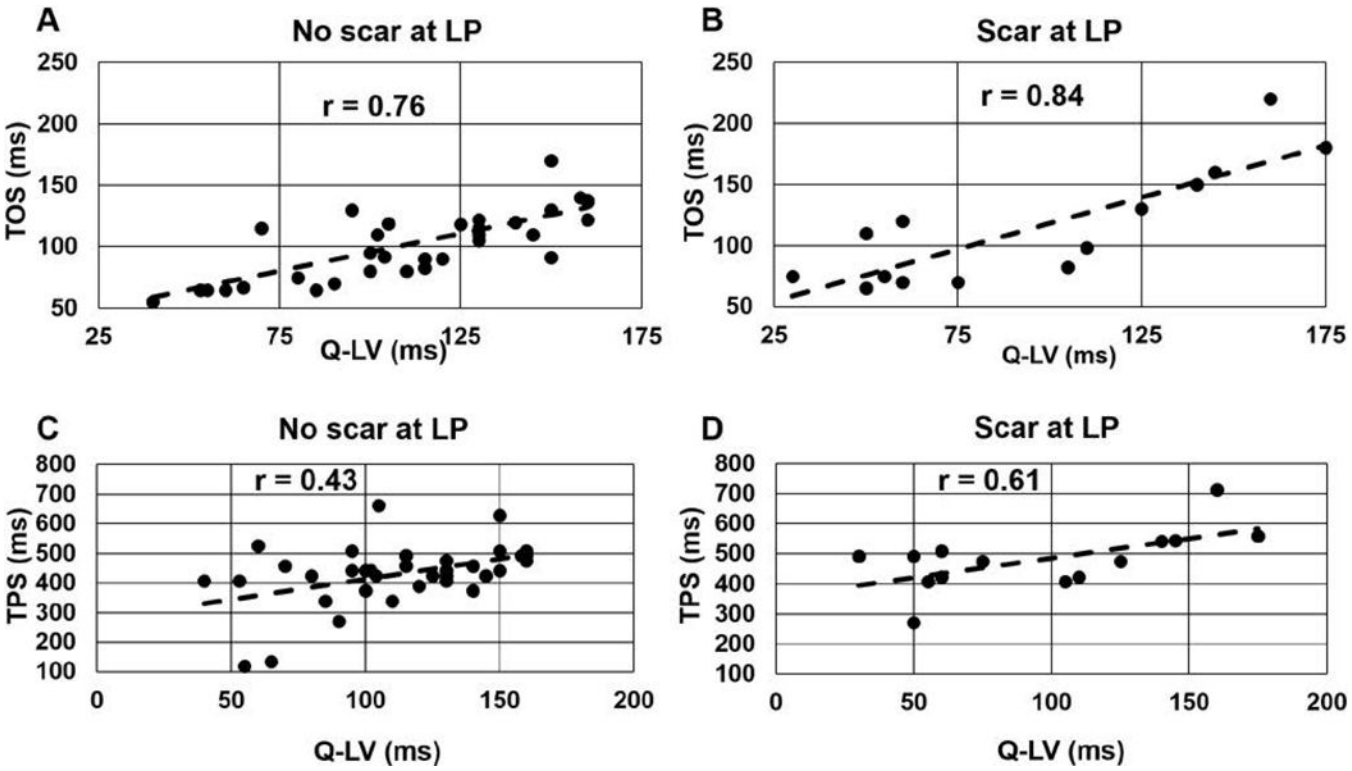

Figure 3. Electromechanical correlations

Correlation plots are shown for: (A) TOS vs. Q-LV for patients with the LV lead location in a region without scar, (B) TOS vs. Q-LV with the LV lead placed in scar, (C) TPS vs. Q-LV for LV lead implant sites without scar, and (D) TPS vs. Q-LV LV lead implant sites with scar.

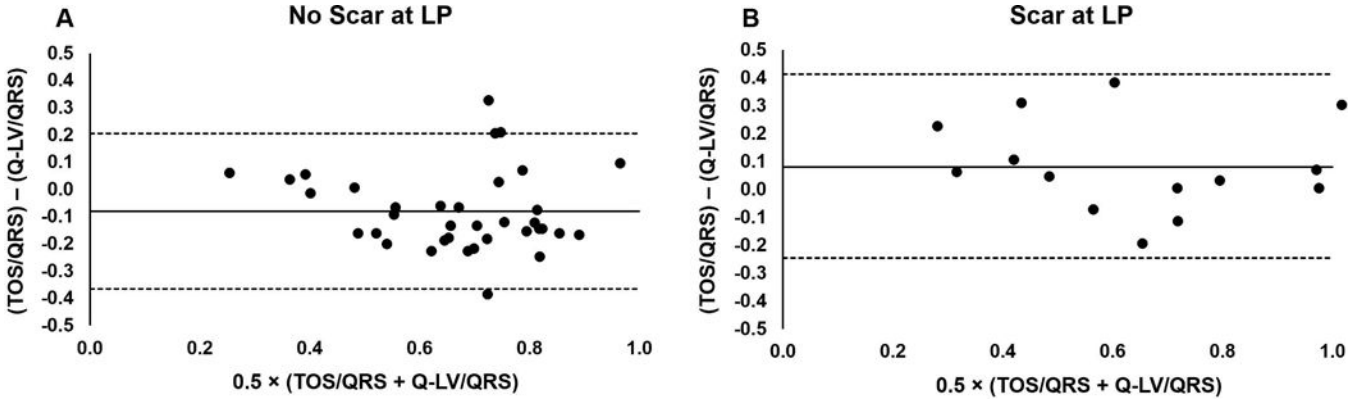

Figure 4. Electromechanical Bland-Altman analysis

Bland-Altman plots are shown to assess the agreement between TOS/QRS and QLV/QRS for the cases of (A) patients with the LV lead location in a region without scar, and (B) cases with the LV lead placed in scar. In both cases, fairly small biases are observed, with a greater delay in mechanical activation relative the electrical activation when the LV lead was placed in a region with scar.

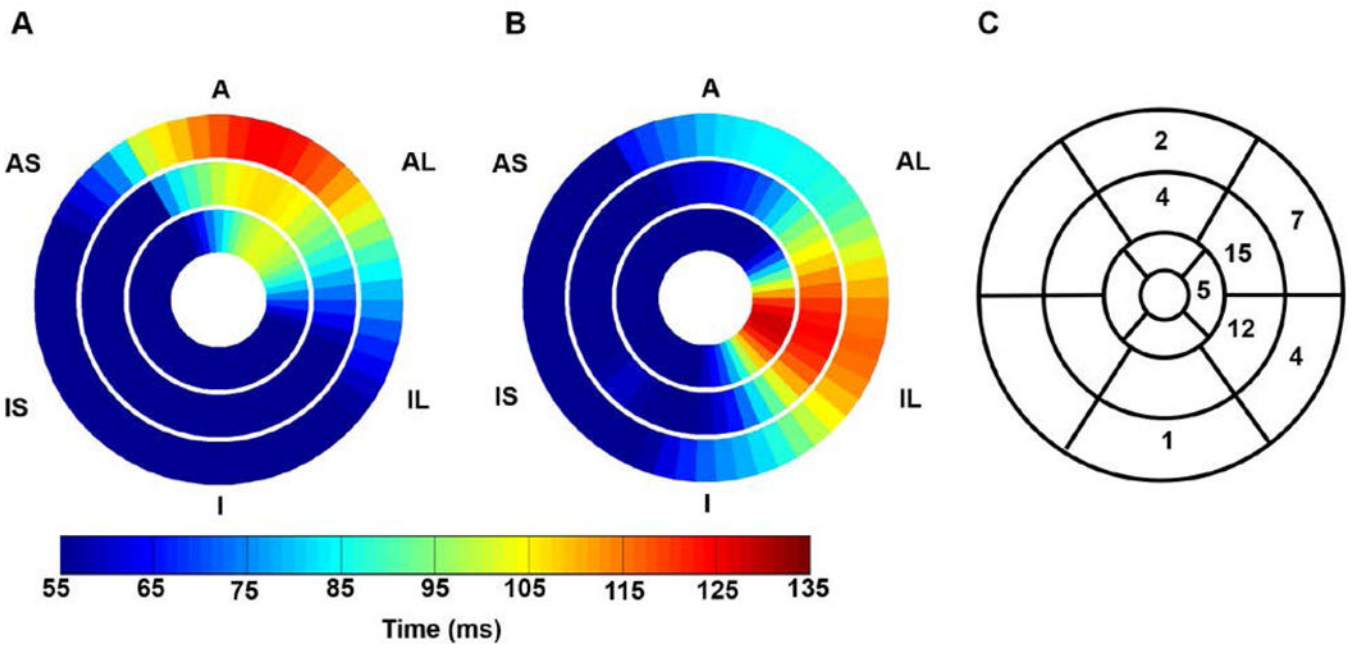

Figure 5. Heterogeneity of the location of the latest mechanically activated segment

(A) An example patient is shown with the latest mechanical activation in the basal anterior segment of the LV. (B) An example patient is shown with latest mechanical activation occurred in the apical inferolateral segment. (C) The distribution of the location of the latest activated segments is shown for all patients.

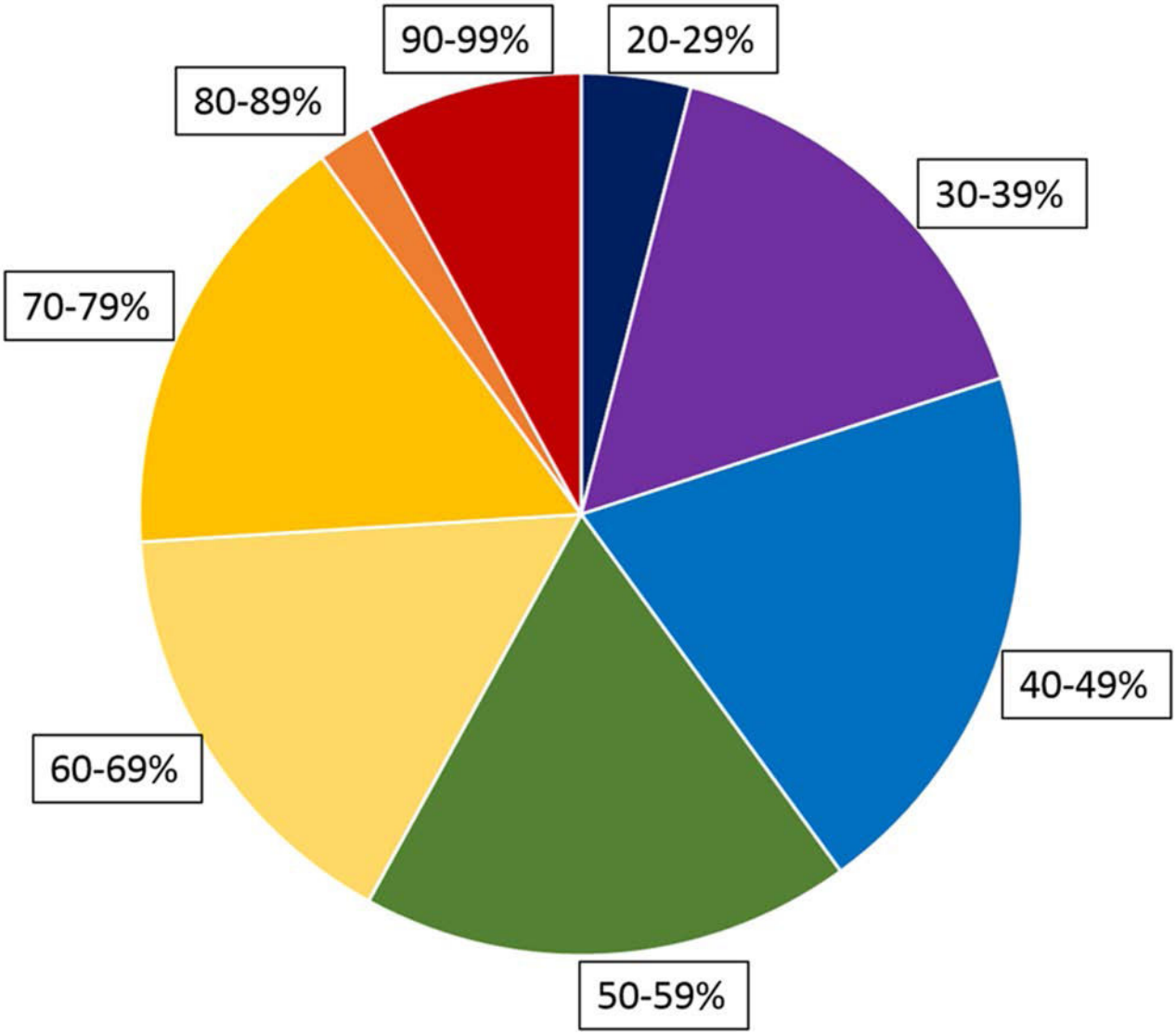

Figure 6. Frequency of LV lead implantation in late-activation sites with the standard CRT procedure

The time to the onset of shortening (TOS) has been normalized to the QRS duration to specify activation time as a percentage of the QRS width. In more than half the patients undergoing CRT, the LV lead was placed in a region with TOS less than 60% of the QRS duration.

Table 1

Clinical and MRI Characteristics of CRT Cohort (n=50)

Characteristics	
Age (years)	64.8 ± 9.6
Gender (female)	15 (30%)
Ischemic Heart Disease (n [%])	26 (52%)
Diabetes Mellitus (n [%])	18 (36%)
CKD (n [%])	13 (26%)
RBBB (n [%])	3 (6%)
NYHA Class	
NYHA II (n [%])	9 (18%)
NYHA III (n [%])	41 (82%)
CRT Indication	
QRS Duration (ms)	159 ± 18.2
Class I (LBBB, QRS ≥ 150 ms) (n [%])	32 (64%)
Class IIa (n [%])	18 (36%)
Medications	
Beta Blocker (n [%])	47 (94%)
Carvedilol (n [%])	25 (50%)
Metoprolol (n [%])	22 (44%)
ACEI OR ARB (n [%])	47 (94%)
ACE Inhibitor (n [%])	40 (80%)
ARB (n [%])	7 (14%)
Loop Diuretic (n [%])	39 (78%)
Spironolactone (n [%])	17 (34%)
Digoxin (n [%])	4 (8%)
Anticoagulant (n [%])	12 (24%)
Warfarin (n [%])	7 (14%)
Novel Anticoagulant (NOAC) (n [%])	5 (10%)
Cardiac MR Characteristics	
LVESVI (ml/m^2)	127.8 ± 39.9
LVEDVI (ml/m^2)	102.5 ± 36.3
SVI (ml/m^2)	30.8 ± 10.4
LVEF	0.24 ± 0.08
LVMI (g/m^2)	72.8 ± 22.0
CURE	0.59 ± 0.23

Table 2

Bivariable Linear Associations Between MRI Parameters and the Percent Change in LVESV After CRT*

	Beta Coefficient	Standard Error	t Value	P-Value	Standarized Coefficient
CURE-SVD	0.574	0.129	4.45	<.0001	0.540
TOS	−0.00237	0.000968	−2.44	0.018	−0.333
TOS/QRS	−0.461	0.177	−2.60	0.012	−0.352
Time to Peak Contraction	0.0000176	0.000337	0.05	0.96	0.00754
Scar at LV Pacing Site	0.186	0.0711	2.62	0.012	0.353

* The beta coefficients and p-values in each row refer to separate bivariable (also called bivariate) linear models with the percent change in LVESV as the dependent variable and the MRI parameter listed in the row as the independent variable. For example, the beta coefficient in row 2 for TOS refers to the linear model evaluating the relationship between TOS and the percent change in LVESV.

Table 3

Multivariable Linear Model for Percent Change in LVESV Post-CRT with TOS

Covariate	Beta Coefficient	Standard Error	t Value	P-Value	Standardized Coefficient
Intercept	−0.259	0.116	−2.24	0.030	0
CURE-SVD	0.470	0.123	3.82	0.0004	0.442
TOS/QRS Duration	−0.433	0.145	−2.98	0.0046	−0.331
LV Pacing Site in Scar	0.127	0.0609	2.09	0.042	0.242

*R^2=0.44 for model

Table 4

Multivariable Linear Model for Percent Change in LVESV Post-CRT with TPS

Covariate	Beta Coefficient	Standard Error	t Value	P-Value	Standardized Coefficient
Intercept	−0.426	0.160	−2.66	0.011	0
CURE-SVD	0.511	0.133	3.84	0.0004	0.481
TPS	−0.000201	0.000286	−0.70	0.49	−0.086
LV Pacing Site in Scar	0.120	0.0671	1.80	0.079	0.229

*R^2=0.34 for model